Nonrelativistic Spin-Momentum Coupling in Antiferromagnetic Twisted Bilayers

Ran He,[1] Dan Wang,[2] Nannan Luo,[1] Jiang Zeng,[1] Ke-Qiu Chen,[1] and Li-Ming Tang[1,*]
[1]Department of Applied Physics, School of Physics and Electronics, Hunan University, Changsha 410082, China
[2]Institute of Mathematics and Physics, Central South University of Forestry and Technology, Changsha 410018, China

(Received 26 April 2022; revised 1 June 2022; accepted 5 January 2023; published 25 January 2023)

Spin-momentum coupling, which depends strongly on the relativistic effect of heavy elements in solids, is the basis of many phenomena in spintronics. In this Letter, we theoretically predict nonrelativistic spin-momentum coupling in two-dimensional materials. By proposing magnetic symmetry requirements for spin splitting in two-dimensional systems, we find that a simple twisting operation can realize nonrelativistic spin splitting in antiferromagnetic bilayers. Through first-principles calculations, we demonstrate that momentum-dependent spin splitting exists extensively in antiferromagnetic twisted bilayers with different crystal structures and twist angles. The size of the spin splitting caused by twisting is of the same order of magnitude as that arising from spin-orbit coupling. In particular, a transverse spin current with an extremely high charge-spin conversion ratio can be generated in twisted structures under an external electric field. The findings demonstrate the potential for achieving electrically controlled magnetism in materials without spin-orbit coupling.

DOI: 10.1103/PhysRevLett.130.046401

Energy bands with momentum-dependent spin splitting enable spintronic applications [1,2]. In previous studies on spin-momentum coupling in materials with zero net magnetization, the spin-orbit coupling (SOC) of heavy elements has played an essential role [3]. However, the rapid decoherence and relatively short diffusion length of spin-polarized electrons induced by SOC limit the applications of these materials [4]. In addition, the rarity, instability, and toxicity of materials incorporating heavy elements also highlight the need for an alternative strategy to realize spin-momentum coupling in the absence of SOC.

Antiferromagnetic (AFM) materials have attracted considerable research interest due to their robustness, ultrafast dynamics, and magnetotransport effects [5]. Recent studies have suggested that nonrelativistic spin-momentum coupling can be realized in some unconventional AFM materials [6–9] due to the absence of combined symmetry of time reversal, inversion, and translation [7,10]. In these unconventional AFM materials, the spin momentum-coupled band structure is usually accompanied by spin currents flowing transverse to the external electrical field, similar to the spin Hall effect [11]. Based on this effect, spin-splitter torque (SST), a new type of spin torque that combines the advantages of conventional spin-transfer torque and spin-orbit torque, was theoretically proposed [12] and subsequently observed experimentally [13,14].

However, antiferromagnetism-induced spin-momentum coupling has not been reported in two-dimensional (2D) van der Waals (vdW) materials, which exhibit diverse electronic properties and excellent tunability [15,16]. Since the experimental discovery of 2D magnetic ordering, 2D magnetic materials have become a hot topic of scientific research as promising candidates for next-generation information [17–19]. Although common 2D collinear AFM materials exhibit no nonrelativistic spin splitting, there are numerous ways to tune the properties of 2D vdW materials due to their unique vdW-type interlayer interactions. Among the proposed methods, the manipulation of electronic structures by twisting vertically stacked vdW structures has attracted intense interest [20–23]. Twisted systems consisting of magnetic 2D layers have been extensively studied due to their novel properties, which include magnetic ground states [24], multiflavor magnetic states [25], noncollinear magnetic states [26], and Moiré magnon bands [27].

In this Letter, we discuss the realization of nonrelativistic spin-momentum coupling in 2D systems. Based on a consideration of magnetic symmetry expanded from three-dimensional (3D) cases, we found that simple twisting, which receives considerable attention in 2D systems, may be a new strategy for generating nonrelativistic spin-momentum coupling in AFM bilayers. We performed first-principles calculations of 2D transition metal halide $NiCl_2$ bilayer systems as typical examples. For normally stacked AFM bilayers, the spin is degenerate in the band structure. Interestingly, when there is a twist between the two layers, the decrease in symmetry leads to a large k-dependent spin splitting. Further calculations demonstrated that this nonrelativistic spin-momentum coupling exists universally in twisted bilayer systems with interlayer AFM coupling. Moreover, an external electric field can induce both transverse and longitudinal spin-polarized current in such twisted AFM bilayers due to the different principal axes of the two anisotropic spin electrons.

In crystals, the spin degeneracy is preserved by magnetic symmetries. The energy dispersion $E(k,\sigma)$ is transferred under symmetry operations: a time reversal ($\mathcal{T}$) that reverses both the wave vector k and the spin σ leads to $\mathcal{T}E(k,\sigma) = E(-k,-\sigma)$; a spatial inversion ($\mathcal{I}$) that reverses k but keeps σ invariant results in $\mathcal{I}E(k,\sigma) = E(-k,\sigma)$; and a spatial translation (t) that has no impact on the energy dispersion leaves $tE(k,\sigma) = E(k,\sigma)$. If the system is invariant under the combination of $\mathcal{I}\mathcal{T}t$ operation, the energy dispersion of the system satisfies $E(k,\sigma) = \mathcal{I}\mathcal{T}tE(k,\sigma) = E(k,-\sigma)$, and the two spin subbands remain degenerate in the entire reciprocal space. When SOC is not considered, there is the spinor reversal (U) operation. Unlike $\mathcal{T}$, which reverses the directions of all movements, U simply reverses the signs of the spin and magnetic moments: $UE(k,\sigma) = E(k,-\sigma)$. For the same reason, Ut symmetry also ensures double spin degeneracy for arbitrary wave vectors. Therefore, SOC-unrelated spin splitting in 3D systems requires violations of $\mathcal{I}\mathcal{T}t$ and Ut symmetry [7,10].

For 2D systems, violations of the above two symmetries are insufficient to realize spin splitting. Unlike 3D materials, the wave vector k in 2D systems has only in-plane components. Therefore, the energy dispersion in a 2D system remains unchanged under planar mirror reflection ($\mathcal{M}$): $\mathcal{M}E(k,\sigma) = E(k,\sigma)$. Thus, the realization of spin splitting in 2D systems requires violations of (i) $\mathcal{I}\mathcal{T}t$ symmetry, (ii) $\mathcal{M}\mathcal{I}\mathcal{T}t$ symmetry, (iii) Ut symmetry, and (iv) $\mathcal{M}Ut$ symmetry. In other words, spin splitting is not allowed to exist in 2D antiferromagnets when the two spin sublattices can be transposed onto each other by inversion, translation, planar mirror reflection, or their combination.

Because of the additional restriction from the symmetry consideration, it is even more difficult to realize sufficiently large spin splitting in AFM 2D systems compared to in their 3D counterparts. We theoretically analyzed well-studied inorganic 2D magnetic materials [16], including binary transition metal halides (e.g., $NiCl_2$ and CrI_3), binary transition metal chalcogenides (e.g., VSe_2) and MXenes (e.g., MnB), other binary transition metal compounds (e.g., Co_2P), ternary transition metal compounds (e.g., $MnBi_2Te_4$), and p/f magnets (e.g., K_2N). Different stackings and all three AFM configurations were also considered: G type (both intraplane and interplane couplings are AFM), A type [intraplane coupling is ferromagnetic (FM), while interplane coupling is AFM], and C type (intraplane coupling is AFM, while interplane coupling is FM). Symmetry analysis and calculations verified the absence of any significant nonrelativistic spin splitting in most typical 2D collinear AFM materials.

For bilayer systems with interlayer antiferromagnetism, it is difficult to violate these four symmetries simultaneously using ordinary stacking methods. Consider the tetragonal (1T) transition metal halides and chalcogenides (Fig. 1), which are 2D magnetic materials with the most common structures. For the AA stacking order, the top and bottom layers with opposite magnetic moments can be transposed onto each other via inversion. Thus, the spin degeneracy is preserved by the $\mathcal{I}\mathcal{T}t$ symmetry (the translation is a zero vector). For the AA^R stacking order, although the $\mathcal{I}\mathcal{T}t$ symmetry is broken, the Umt symmetry appears. When there is a twist between the two layers, the top and bottom layers cannot be transposed onto each other in the absence of π rotations about the [110], [2–10], or [−120]. Thus, the above four symmetries are broken, and spin splitting is expected in the twisted bilayer.

Here, we use $NiCl_2$ as an example to demonstrate the above proposal in detail. The vdW material $NiCl_2$ has been widely studied theoretically and experimentally [28–30]. The stable, minimum-energy 1T structure of $NiCl_2$ is semiconducting with a magnetic moment of ∼2 μB per Ni atom and shows weak interlayer AFM coupling. Twisted-bilayer $NiCl_2$ is constructed following the standard commensuration method. The atomic structure of the Moiré

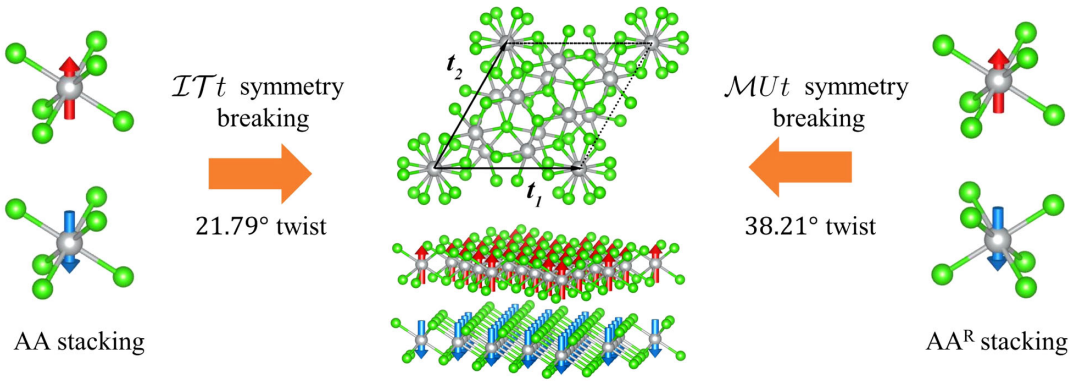

FIG. 1. Crystal and magnetic structures of bilayers constructed by 1T-phase 2D vdW materials with different stacking methods. Red and blue arrows indicate the local magnetic moments of magnetic ions. Double spin degeneracy is preserved by $\mathcal{I}\mathcal{T}t$ symmetry for the AA stacking configuration and $\mathcal{M}Ut$ symmetry for the AA^R stacking configuration. A twisting operation can break these two symmetries, resulting in spin splitting unrelated to SOC.

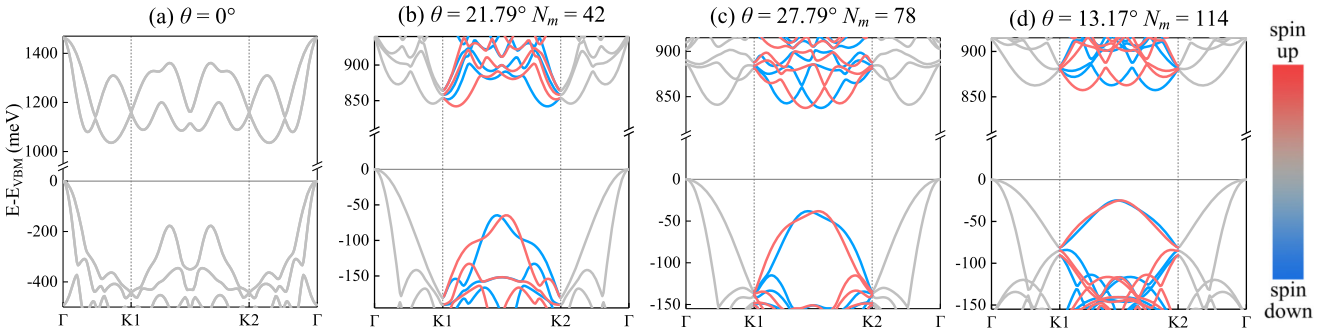

FIG. 2. Band structures of interlayer AFM bilayer $NiCl_2$ with different twist angles θ and numbers of atoms N_m: (a) $\theta = 0°$, $N_m = 6$; (b) $\theta = 21.79°$, $N_m = 42$; (c) $\theta = 27.79°$, $N_m = 78$; and (d) $\theta = 13.17°$, $N_m = 114$. The path between $K_1(\frac{2}{3}, \frac{1}{3})$ and $K_2(-\frac{1}{3}, \frac{1}{3})$ is not a high-symmetry path.

superlattice with twist angle $\theta = 21.79°$ is shown in Fig. 1. For a $NiCl_2$ monolayer, the atomic structure possesses threefold rotational symmetry. Thus, the twisted bilayer with $0° < \theta < 60°$ is symmetrically the same as the bilayers with $60° < \theta < 120°$. The twisted-bilayer superlattices with a number of atoms $N_m < 120$ ($\theta = 13.17°$, 21.79°, 27.79°, 32.21°, 38.21°, and 46.83°) were investigated. To determine the most preferred magnetic ordering, we compared the bilayers with interlayer FM coupling and interlayer AFM coupling and calculated the exchange energy as $E_{ex} = E_{FM} - E_{AFM}$. All structures were found to have positive exchange energy [31], indicating that interlayer AFM coupling is more stable than FM coupling in these twisted $NiCl_2$ bilayers.

We then compared the electronic structures of the ordinarily stacked $NiCl_2$ bilayer (without interlayer twisting) and the twisted bilayers. The negligible SOC was not considered. The calculations indicated that all the structures with interlayer AFM order are stable. Similar to conventional antiferromagnets, the two spin bands of the untwisted bilayer are entirely coincidental in the whole Brillouin zone [Fig. 2(a)]. In contrast, significant splitting between the two spin subbands appears in all the twisted bilayer systems with different twist angles [Figs. 2(b), 2(c), and 2(d)]. Unlike spin splitting in FM materials, this spin splitting in AFM materials is dependent on the wave vector.

The 3D band structure and color map [Figs. 3(a) and 3(b)] clearly illustrate the distribution of spin splitting between pairs of bands in reciprocal space. The spin splitting appears at ordinary k points but not at high-symmetry points and paths. Along the Γ–K_1 paths, for example, $\mathcal{T}\{C_{2a}|0\}$ keeps k invariant and transfers the spin state to the opposite spin state, thereby enforcing degeneracy between them. Here, C_{2a} is the π rotation about the [−120] axes. In contrast, there is no such symmetry for ordinary k points, and spin splitting is expected at these ordinary k points. It should be noted that the sum of the spin splitting magnitude over the entire Brillouin zone vanishes because the spin splitting is antisymmetric under mirror reflection in reciprocal space.

The induction of spin splitting upon twisting a bilayer system with interlayer AFM coupling is a universal phenomenon. As for 1T-phase $NiCl_2$, spin splitting might also be found in Moiré superlattices constructed from other

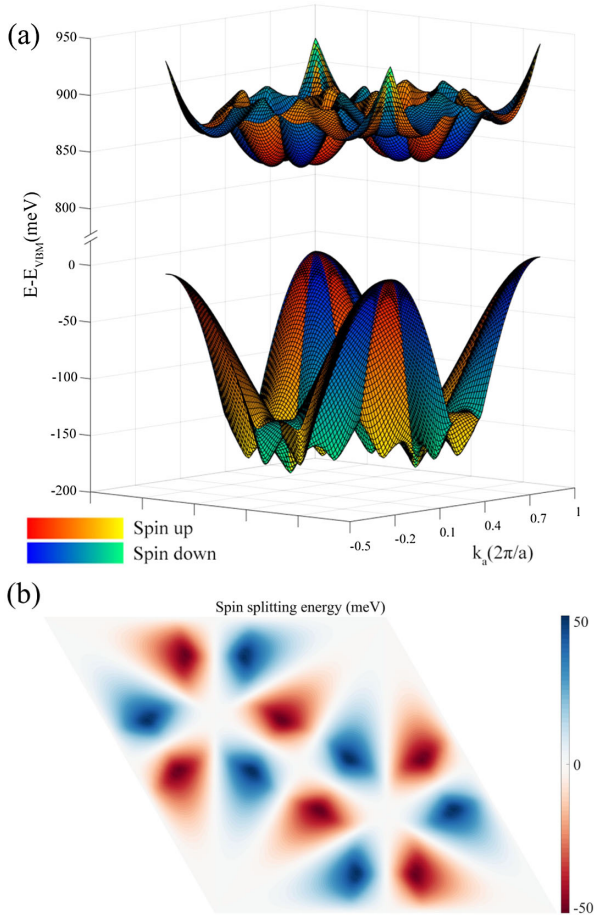

FIG. 3. (a) 3D band structures of the valence and conduction bands and (b) spin splitting distribution $E_{up}(k) - E_{down}(k)$ of the valence band in interlayer AFM twisted bilayer $NiCl_2$ with $\theta = 21.79°$. The intensity of color in (a) reflects the distance to the Fermi level.

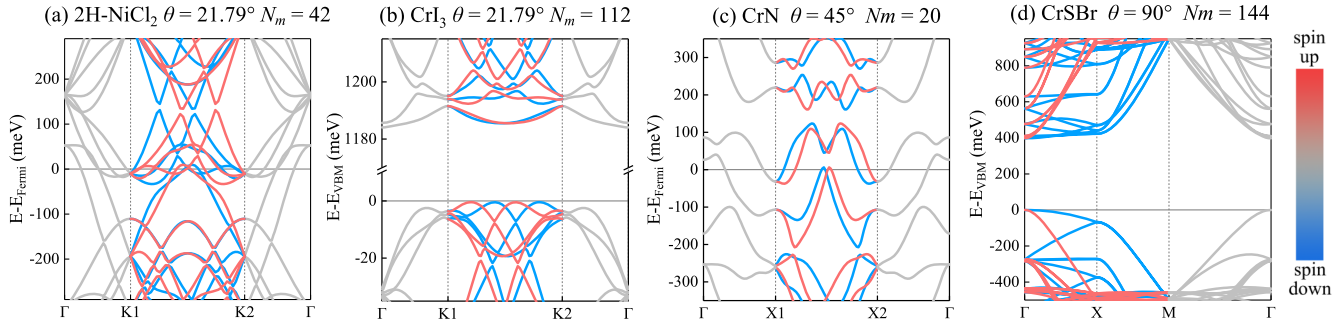

FIG. 4. Spin splitting in interlayer AFM twisted bilayers constructed from 2D materials with different crystal structures: (a) 2H-phase $NiCl_2$; (b) CrI_3 with a hexagonal lattice where $M_1 = (\frac{1}{2}, 0)$ and $M_2 = (\frac{1}{2}, \frac{1}{2})$; (c) CrN with a square lattice where $X_1 = (\frac{1}{2}, 0)$ and $X_2 = (0, \frac{1}{2})$; and (d) CrSBr with a rectangular lattice. The corresponding crystal and magnetic structures are shown in the Supplemental Material [31].

2D materials with different crystal structures, such as hexagonal (2H) $NiCl_2$ [Fig. 4(a)], CrI_3 [Fig. 4(b)], and CrN [Fig. 4(c)]. A twisted bilayer system with interlayer AMF coupling usually possesses a large magnitude of spin splitting comparable to that of spin splitting resulting from SOC in compounds with heavy atoms. Thus, the spin splitting can be directly measured by spin- and angle-resolved photoemission spectroscopy. In the interlayer AFM twisted bilayer constructed from $NiCl_2$ with $\theta = 21.79°$, the spin splitting of the valence band can reach 50 meV [Fig. 3(b)]. A greater spin splitting magnitude can be achieved in $NiCl_2$ when the two spin sublattices have a larger directional difference around the 30° twist angle. The magnitude of spin splitting also depends on the steepness of the energy band. In twisted $FeCl_2$ or 2H-$NiCl_2$, the magnitude of spin splitting near the Fermi energy can exceed 100 meV.

Furthermore, this kind of spin-momentum coupling could be used to generate spin-polarized current under an external electric field or temperature gradient [8,9,11]. This phenomenon is called the spin-splitter effect [12]. Unlike the anomalous spin Hall effect, the spin-splitter effect is nonrelativistic and unrelated to the Berry curvature. The spin-splitter effect is caused by the different anisotropies of the two spin subbands. The difference between them lies in the spin conductivity tensor σ_{cb}^{a} [12], where a is to the spin polarization of the spin current, b is the direction of spin-current flow, and c is the direction of the applied electric field. The spin conductivity tensor can be divided into two contributions: $\sigma_{cb}^{a} = \sigma_{cb}^{a,\mathrm{odd}} + \sigma_{cb}^{a,\mathrm{even}}$. The odd part corresponds to the contribution from the anomalous spin Hall effect and satisfies $\sigma_{bc}^{a,\mathrm{odd}} = -\sigma_{cb}^{a,\mathrm{odd}}$. The even part corresponds to the contribution of the spin splitting effect and satisfies $\sigma_{cb}^{a,\mathrm{even}} = \sigma_{bc}^{a,\mathrm{even}}$.

The shape of the conductivity tensor is constrained by the crystal symmetry [32,33]. Considering the even conductivity tensor of a 2D material, nonzero off-diagonal elements are not allowed to exist when the crystal has threefold, fourfold, or sixfold rotational symmetry [33]. It means SSE is expected in the AFM twisted bilayers constructed by anisotropic 2D materials. In the AFM bilayer, as shown in Fig. 5(a), the upper and lower layers have different principal axes of anisotropy after twisting. Under an external electric field, the currents of the spin-up and spin-down electrons are not parallel to each other, resulting in a transverse spin current.

Twisted bilayer systems of 2D M-X-Y family materials (M = transition metal; X = O, S, Se, Te; Y = Cl, Br, I) [34], which have only twofold rotational symmetry and anisotropic conductivity, are expected to be appropriate candidates for SSE. Monolayer M-X-Y systems are FM semiconductors with large spin polarization and high Curie temperature. These systems also possess large perpendicular magnetic anisotropy, a wide range of band gaps, high carrier mobility, and large light absorption [16]. Thus, M-X-Y materials show promise for designing high-performance electronic and spintronic devices. Here, we selected 2D CrSBr as a prototype to investigate the spin-polarized current in twisted bilayers. CrSBr monolayer has a rectangular primitive cell with a larger lattice constant in the b axis ($b = 4.76$ Å) than in the a axis ($a = 3.50$ Å) [35]. Monte Carlo simulations demonstrated that the CrSBr system possesses a high Curie temperature of 290 K [36]. A square Moiré superlattice with twist angle $\theta = 90°$ can be constructed from two $4a \times 3b$ CrSBr supercells [31]. The electronic structure of the twisted CrSBr superlattice is shown in Fig. 4(d). The two spin subbands of the twisted CrSBr superlattice have different anisotropies [Fig. 5(b)], resulting in different current directions of the spin-up and spin-down electrons under an electric field.

As shown in Figs. 5(c) and 5(d), a combination of first-principles calculations and semiclassical Boltzmann theory showed that a transverse spin current can be induced by an electric field in interlayer AFM twisted-bilayer CrSBr. The charge-spin conversion ratio largely depends on the direction of the electric field. When the external electric field is parallel to the [110], [$\bar{1}$10], [1$\bar{1}$0], and [$\bar{1}$ $\bar{1}$ 0] crystal

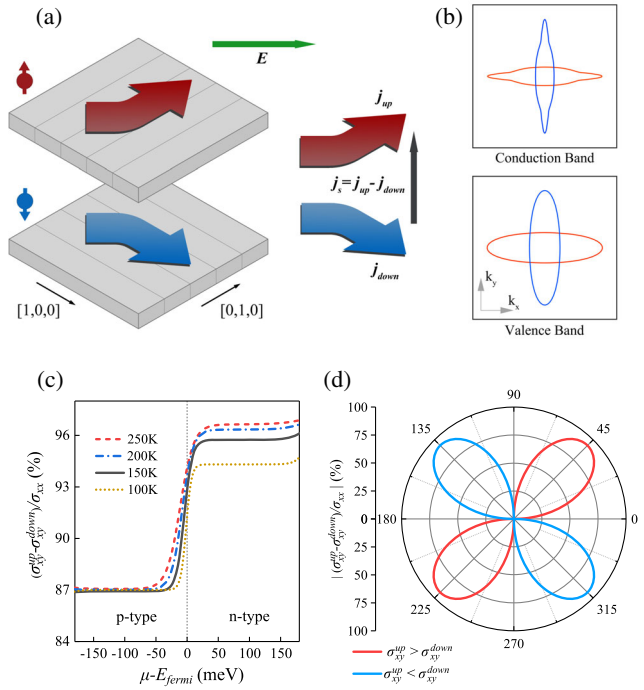

FIG. 5. (a) Schematic of spin current in an AFM twisted bilayer. The two plates denote the twisted bilayer with interlayer AFM order. The lines in the plates indicate the directions of anisotropy. The direction parallel to the lines has the largest conductivity. (b) Energetic contours of the valence and conduction bands. The blue and red lines indicate the two spin components. Top: 40 meV below the valence band maximum. Bottom: 16 meV above the conduction band minimum. (c) Relation between the intrinsic charge-spin conversion ratio and the direction of the electric field (α is the angle between electric field and the [1,0,0] crystal direction) in twisted-bilayer CrSBr with $T = 150$ K. (d) Charge-spin conversion ratio as a function of chemical potential at different temperatures for $\alpha = 45°$.

directions, a pure spin current is perpendicular to the electric field, and the charge-spin conversion ratio is maximized. Here, the charge-spin conversion ratio is defined as the ratio of the longitudinal charge current to the transverse spin current. The charge-spin conversion ratio is expressed as $(\sigma_{xy}^{\mathrm{up}} - \sigma_{xy}^{\mathrm{down}})/\sigma_{xx}$, where x is the direction of the electric field. The intrinsic charge-spin conversion ratio reaches 90%, which is significantly larger than the charge-spin conversion ratios of 3D collinear AFM RuO_2 systems [12] and the widely used spin Hall material Pt [37]. Figure 5(d) shows that both n-type and p-type twisted-bilayer CrSBr systems exhibit high charge-spin conversion ratios at different temperatures. These results demonstrate the possibility of generating SST in 2D materials.

In conclusion, we proposed a novel yet simple strategy to realize spin-momentum coupling by twisting interlayer AFM bilayers. Unlike in 3D systems, the spin degeneracy is preserved by either the $\mathcal{I}t$, $\mathcal{M}\mathcal{I}t$, Ut, or $\mathcal{M}Ut$ symmetry in 2D systems. A twisting operation can break all these symmetries in AFM bilayers to realize nonrelativistic spin splitting. Based on first-principles calculations, we showed that the k-dependent spin splitting can be generated by twisting in common 2D magnetic materials. The amplitude of spin splitting is comparable to that induced by SOC from heavy atoms. Transverse spin-polarized current can be induced under an external electric field in twisted bilayers of anisotropic 2D materials. Using CrSBr as a model, we obtained a maximum transverse charge-spin conversion ratio of 90%, significantly higher than those reported in spin Hall effect materials.

This work was supported by the National Natural Science Foundation of China through Grants No. 12074112, No. 12104516, and No. 11674090.

*lmtang@semi.ac.cn

[1] A. Fert, Rev. Mod. Phys. **80**, 1517 (2008).
[2] I. Žutić, J. Fabian, and S. Das Sarma, Rev. Mod. Phys. **76**, 323 (2004).
[3] A. Manchon, H. C. Koo, J. Nitta, S. M. Frolov, and R. A. Duine, Nat. Mater. **14**, 871 (2015).
[4] A. Manchon, J. Železný, I. M. Miron, T. Jungwirth, J. Sinova, A. Thiaville, K. Garello, and P. Gambardella, Rev. Mod. Phys. **91**, 035004 (2019).
[5] V. Baltz, A. Manchon, M. Tsoi, T. Moriyama, T. Ono, and Y. Tserkovnyak, Rev. Mod. Phys. **90**, 015005 (2018).
[6] T. Berlijn, P. C. Snijders, O. Delaire, H.-D. Zhou, T. A. Maier, H.-B. Cao, S.-X. Chi, M. Matsuda, Y. Wang, M. R. Koehler, P. R. C. Kent, and H. H. Weitering, Phys. Rev. Lett. **118**, 077201 (2017).
[7] L.-D. Yuan, Z. Wang, J.-W. Luo, E. I. Rashba, and A. Zunger, Phys. Rev. B **102**, 014422 (2020).
[8] M. Naka, S. Hayami, H. Kusunose, Y. Yanagi, Y. Motome, and H. Seo, Nat. Commun. **10**, 4305 (2019).
[9] M. Naka, Y. Motome, and H. Seo, Phys. Rev. B **103**, 125114 (2021).
[10] L.-D. Yuan, Z. Wang, J.-W. Luo, and A. Zunger, Phys. Rev. Mater. **5**, 014409 (2021).
[11] L. Šmejkal, R. González-Hernández, T. Jungwirth, and J. Sinova, Sci. Adv. **6**, eaaz8809 (2020).
[12] R. González-Hernández, L. Šmejkal, K. Výborný, Y. Yahagi, J. Sinova, T. C. V. Jungwirth, and J. Železný, Phys. Rev. Lett. **126**, 127701 (2021).
[13] H. Bai, L. Han, X. Y. Feng, Y. J. Zhou, R. X. Su, Q. Wang, L. Y. Liao, W. X. Zhu, X. Z. Chen, F. Pan, X. L. Fan, and C. Song, Phys. Rev. Lett. **128**, 197202 (2022).
[14] S. Karube, T. Tanaka, D. Sugawara, N. Kadoguchi, M. Kohda, and J. Nitta, Phys. Rev. Lett. **129**, 137201 (2022).
[15] C. Tan, X. Cao, X.-J. Wu, Q. He, J. Yang, X. Zhang, J. Chen, W. Zhao, S. Han, G.-H. Nam, M. Sindoro, and H. Zhang, Chem. Rev. **117**, 6225 (2017).
[16] X. Jiang, Q. Liu, J. Xing, N. Liu, Y. Guo, Z. Liu, and J. Zhao, Appl. Phys. Rev. **8**, 031305 (2021).
[17] B. Huang, G. Clark, E. Navarro-Moratalla, D. R. Klein, R. Cheng, K. L. Seyler, D. Zhong, E. Schmidgall, M. A. McGuire, D. H. Cobden, W. Yao, D. Xiao, P. Jarillo-Herrero, and X. Xu, Nature (London) **546**, 270 (2017).

[18] C. Gong, L. Li, Z. Li, H. Ji, A. Stern, Y. Xia, T. Cao, W. Bao, C. Wang, Y. Wang, Z. Q. Qiu, R. J. Cava, S. G. Louie, J. Xia, and X. Zhang, Nature (London) **546**, 265 (2017).
[19] Z. Fei, B. Huang, P. Malinowski, W. Wang, T. Song, J. Sanchez, W. Yao, D. Xiao, X. Zhu, A. F. May, W. Wu, D. H. Cobden, J.-H. Chu, and X. Xu, Nat. Mater. **17**, 778 (2018).
[20] V. Carozo, C. M. Almeida, E. H. M. Ferreira, L. G. Cançado, C. A. Achete, and A. Jorio, Nano Lett. **11**, 4527 (2011).
[21] H. Zhao, Y.-C. Lin, C.-H. Yeh, H. Tian, Y.-C. Chen, D. Xie, Y. Yang, K. Suenaga, T.-L. Ren, and P.-W. Chiu, ACS Nano **8**, 10766 (2014).
[22] J. Wu, X. Zhang, M. Ijäs, W. Han, X.-F. Qiao, X.-L. Li, D.-S. Jiang, A. Ferrari, and P.-H. Tan, Nat. Commun. **5**, 5309 (2014).
[23] H. Kato, N. Itagaki, and H. Im, Carbon **141**, 76 (2019).
[24] Y. Xu, A. Ray, Y.-T. Shao, S. Jiang, K. Lee, D. Weber, J. Goldberger, K. Watanabe, T. Taniguchi, D. Muller, K. Mak, and J. Shan, Nat. Nanotechnol. **17**, 143 (2022).
[25] K. Hejazi, Z.-X. Luo, and L. Balents, Proc. Natl. Acad. Sci. U.S.A. **117**, 10721 (2020).
[26] F. Xiao, K. Chen, and Q. Tong, Phys. Rev. Res. **3**, 013027 (2021).
[27] C. Wang, Y. Gao, H. Lv, X. Xu, and D. Xiao, Phys. Rev. Lett. **125**, 247201 (2020).
[28] J. Y. Ni, X. Y. Li, D. Amoroso, X. He, J. S. Feng, E. J. Kan, S. Picozzi, and H. J. Xiang, Phys. Rev. Lett. **127**, 247204 (2021).
[29] Y. Rosenfeld Hacohen, R. Popovitz-Biro, E. Grunbaum, Y. Prior, and R. Tenne, Adv. Mater. **14**, 1075 (2002).
[30] Z. Luo, X. Lin, L. Tang, Y. Feng, Y. Gui, J. Zhu, W. Yang, D. Li, L. Zhou, and L. Fu, ACS Appl. Mater. Interfaces **12**, 34755 (2020).
[31] See Supplemental Material at http://link.aps.org/supplemental/10.1103/PhysRevLett.130.046401 for computational methods, crystal structures, magnetic properties, detailed analysis for spin splitting and spin current, and experimental realizability, which include Refs. [38–50].
[32] W. H. Kleiner, Phys. Rev. **142**, 318 (1966).
[33] M. Seemann, D. Ködderitzsch, S. Wimmer, and H. Ebert, Phys. Rev. B **92**, 155138 (2015).
[34] N. Miao, B. Xu, L. Zhu, J. Zhou, and Z. Sun, J. Am. Chem. Soc. **140**, 2417 (2018).
[35] E. J. Telford, A. H. Dismukes, K. Lee, M. Cheng, A. Wieteska, A. K. Bartholomew, Y.-S. Chen, X. Xu, A. N. Pasupathy, X. Zhu, C. R. Dean, and X. Roy, Adv. Mater. **32**, 2003240 (2020).
[36] Z. Jiang, P. Wang, J. Xing, X. Jiang, and J. Zhao, ACS Appl. Mater. Interfaces **10**, 39032 (2018).
[37] J. Sinova, S. O. Valenzuela, J. Wunderlich, C. H. Back, and T. Jungwirth, Rev. Mod. Phys. **87**, 1213 (2015).
[38] P. E. Blöchl, Phys. Rev. B **50**, 17953 (1994).
[39] J. P. Perdew, K. Burke, and M. Ernzerhof, Phys. Rev. Lett. **77**, 3865 (1996).
[40] G. Kresse and J. Furthmüller, Phys. Rev. B **54**, 11169 (1996).
[41] S. L. Dudarev, G. A. Botton, S. Y. Savrasov, C. J. Humphreys, and A. P. Sutton, Phys. Rev. B **57**, 1505 (1998).
[42] G. K. Madsen and D. J. Singh, Comput. Phys. Commun. **175**, 67 (2006).
[43] K. Momma and F. Izumi, J. Appl. Crystallogr. **44**, 1272 (2011).
[44] M. Blei, J. Kapeghian, R. Banerjee, P. Kolari, B. Povilus, Y. Attarde, A. S. Botana, and S. Tongay, Phys. Rev. Mater. **6**, 084003 (2022).
[45] S. Fan, Q. A. Vu, M. D. Tran, S. Adhikari, and Y. H. Lee, 2D Mater. **7**, 022005 (2020).
[46] Y. Huang *et al.*, Nat. Commun. **11**, 2453 (2020).
[47] S. N. P. Wissing, A. B. Schmidt, H. Mirhosseini, J. Henk, C. R. Ast, and M. Donath, Phys. Rev. Lett. **113**, 116402 (2014).
[48] C. Jozwiak, J. A. Sobota, K. Gotlieb, A. F. Kemper, C. R. Rotundu, R. J. Birgeneau, Z. Hussain, D.-H. Lee, Z.-X. Shen, and A. Lanzara, Nat. Commun. **7**, 13143 (2016).
[49] D. MacNeill, G. M. Stiehl, M. H. D. Guimaraes, R. A. Buhrman, J. Park, and D. C. Ralph, Nat. Phys. **13**, 300 (2017).
[50] T. Nan *et al.*, Nat. Commun. **11**, 4671 (2020).